

# 2D Thermo-Structural Code Development for Regenerative Combustion Chamber Analysis

*A. Terracciano, D. Liuzzi, A. Pascucci*

*AVIO S.p.A., Italy, 00034, Colleferro (Rome), Via Latina snc (SP 600 Ariana Km. 5.2)*

## Abstract

In the frame of research activities, AVIO S.p.A. is striving for high effort to design regenerative cooled combustion chamber for the new cryogenic engines development for Vega-E application.

The dimensioning of a regenerative cooled combustion chamber depends on the coupling between the performance of the cooling system and its structural resistance. To optimize the geometry of combustion chamber liner and reduce the design time, a suitable tool is needed to estimate the distribution of temperatures within the wall and the thermo-mechanical stresses that act on the structure.

This objective can be achieved by means of a 3D FEM commercial tool, but a lot of time is needed to perform the geometry by CAD and to set the mesh, boundary condition and execution. Moreover, the process is not automatic, so it is not suitable for an optimization activity of the combustion chamber. To face the challenges of the scope, AVIO S.p.A. developed a 2D tool. The steady state non-linear thermo-structural code is based on finite element method and it is able to analyze typical 2D combustion chamber cross sections and to estimate the temperature field as well as the stress field within the structures. The implementation of input, together with the execution of the code and getting results, require less than 2 orders of magnitude with respect to 3D FEM commercial tool analysis. So, the process is suitable for designing optimization activities, being able to drastically decrease the design time with respect to that required by a 3D FEM commercial tool. The definition of a first geometry of the most representative chamber cross sections, already optimized by the thermo – structural point of view and with respect to number of life cycles required, will be already accomplished. In this way, the 3D – FEM analysis will require 1 or 2 loop as maximum (instead of 5-6 loops required by an optimization activities of the geometry), to analyze only the combustion chamber interfaces.

## 1. Introduction

The designing of regenerative combustion chamber walls for expander cycle engines applications, represents one of the major issue to be faced in the thrust chamber definition. The dual need to chill down the chamber walls due to high temperature reached by gas products, and to guarantee the correct heating of coolant propellant for turbine enthalpy requirement, make the chamber wall thickness dimensioning a crucial point of the design process. To face this issue an optimization activity is required. To accomplish the aim of the cooling system, the chamber walls have to withstand the high values of thermo-mechanical stresses induced into the material.

The figure below shows a cut through the liner with the typical failure mechanism, the dog-house effect.

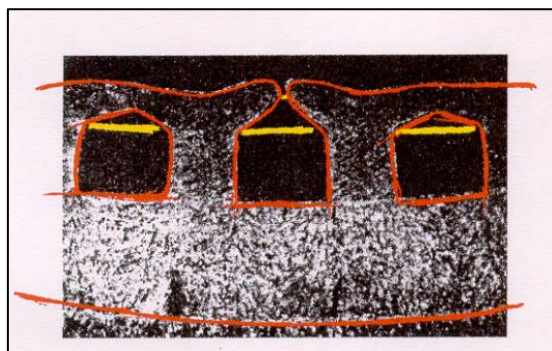


Figure 1: Typical cooling channel failure mode [1]

The tool developed by AVIO (TS\_Code) is based on finite element analysis, and it has been developed to estimate the thermo-mechanical stresses within a typical chamber cross section and to conduct an optimization activity to detect proper walls dimensions in few time, so that to overcome the limits currently imposed by commercial thermo-structural software that are not suitable for an optimization activity.

This work has the scope to compare the results obtained up to now with those provided by commercial software (Marc) in order to investigate the reliability of the TS\_code.

## 2. General Approach

The model generally used to analyze preliminarily the structural robustness of the combustion chamber (see left side of Figure 2) under generalized load conditions (mechanical and thermal loads) is based on the unsteady study of a 2D combustion chamber cross section (see right side of Figure 2) by means of finite elements method analysis.

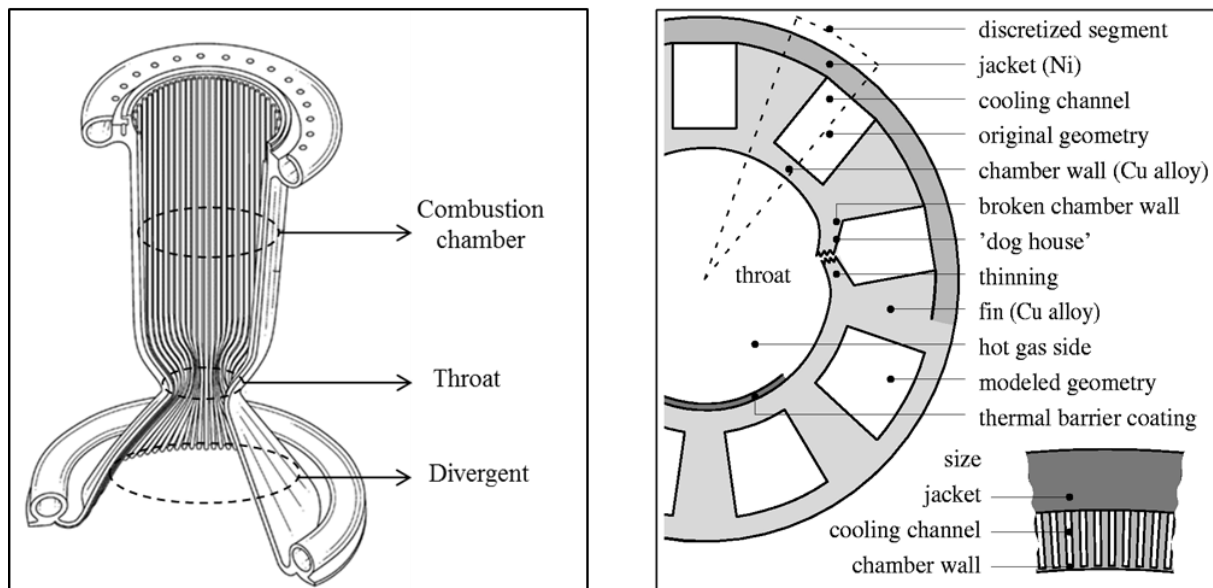


Figure 2: Typical configuration of combustion chamber with three main representative sections (left side). Typical configuration of combustion chamber cross section (right side) [1]

As it is noted by the literature [1][2], this is a feasible approach due to the shape of the combustion chambers. In fact, by adopting the plane strain hypothesis, a study of a 3D elongated body (as the combustion chamber is) by means of 2D representative cross section slice can be conducted with negligible lost in the accuracy of the solution, by imposing symmetric boundary conditions both at right and left side of the slice.

### 2.1 TS\_code Model

In the process of code development, AVIO faced the problem with a simplified approach with respect to the general one. The following simplifications have been involved:

- Stationary Analysis;
- Linear Analysis: no plasticity effect is included;
- The real cross section (here it will be called "Shaped O") has been replaced by a rectangular shaped cross section, "Shaped C" (see Figure 3);

For what concern the boundary conditions, proof test and firing test conditions have been simulated. Both were based on fixed conditions at top side of the cross section analyzed (see Figure 4 – 5 for the differences between the Shaped O geometry boundary conditions and those of Shaped C). In the figures below  $R_1$  and  $R_4$  represent respectively the combustion chamber and the close-out radius, while  $R_2$  and  $R_3$  are the liner and rib radii. Thick1 is equal to  $\frac{1}{2}$  Rib Thickness while Thick2 is the Cooling Channel Thickness at the basis of the channel.

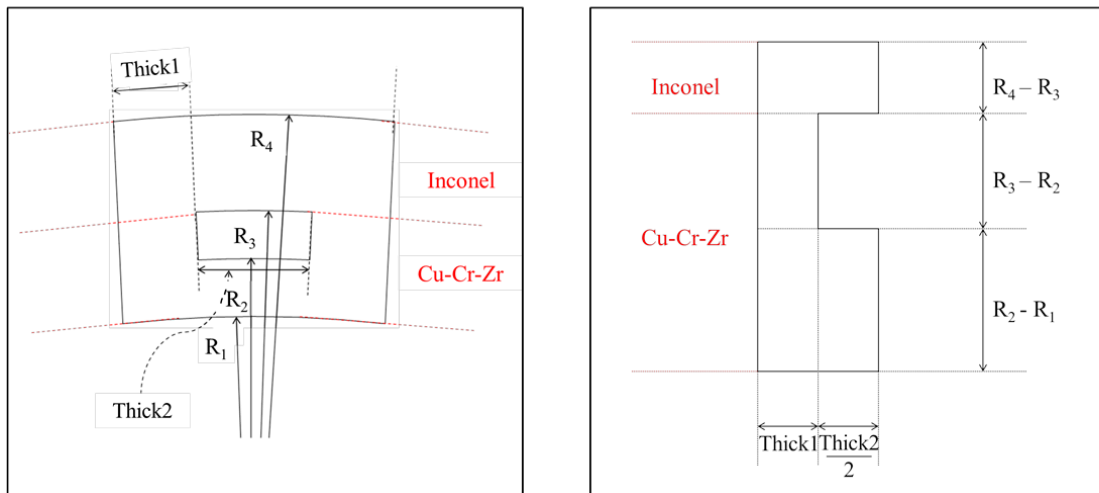


Figure 3: Typical configuration of combustion chamber cross section, Shaped O (left side), and the simplified geometry used in the TS\_code, Shaped C (right side)

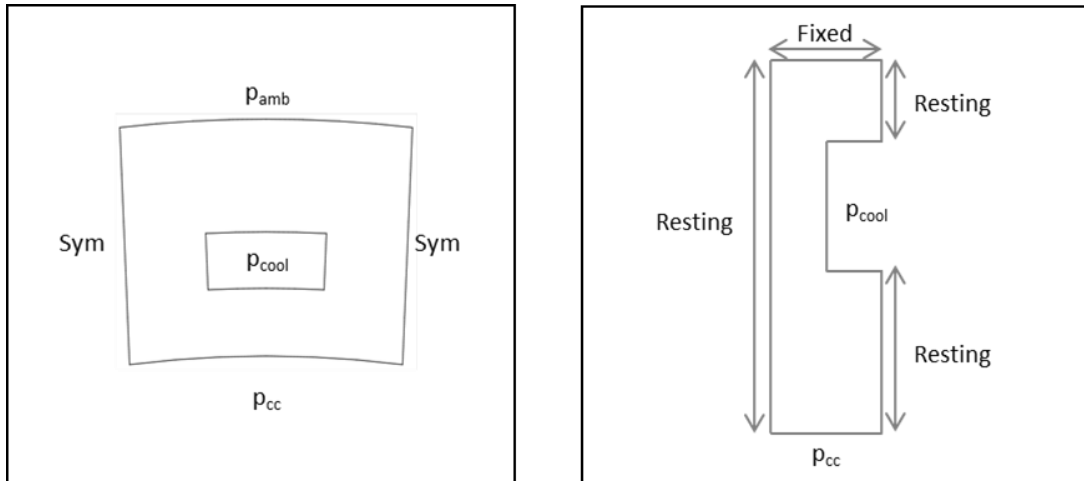


Figure 4: Proof Test conditions for a typical configuration of combustion chamber cross section, Shaped O (left side), and for the simplified geometry used in the TS\_code, Shaped C (right side)

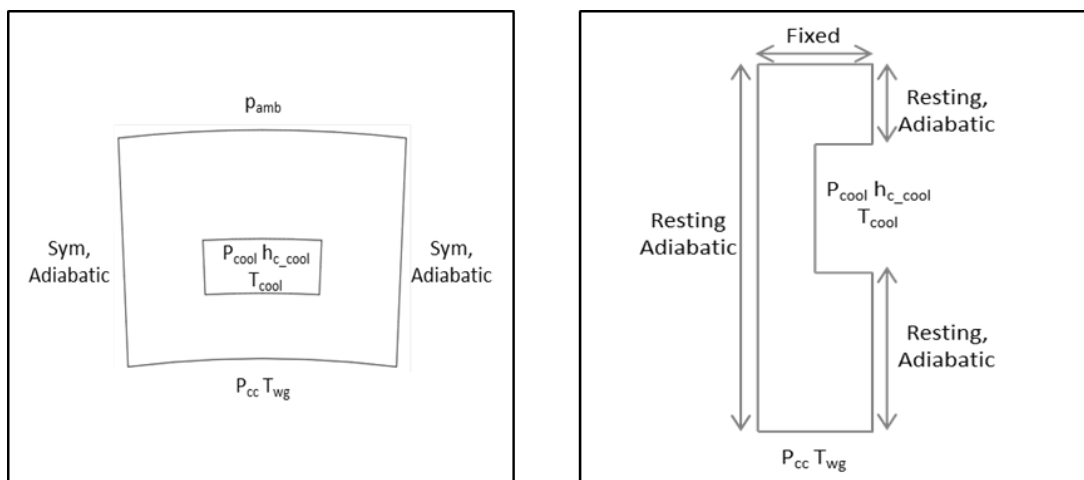


Figure 5: Firing Test conditions for a typical configuration of combustion chamber cross section, Shaped O (left side), and for the simplified geometry used in the TS\_code, Shaped C (right side)

## 2.2 Resolution strategy for Thermo-mechanical problem

The research activity has been based on several steps to accomplish the aim of the problem.

The thermo-structural problem solution was obtained by consecutive analysis of the following sub problems:

- 1D stationary thermo-fluid-mechanical analysis of the system hot gas / combustion chamber wall / coolant;
- 2D thermal analysis of the combustion chamber wall during the hot run;
- 2D linear thermo-structural analysis of the combustion chamber wall under thermal and mechanical loading;

For this study, some of the inputs (such as heat flux coefficient, hot wall temperature, etc.) obtained by the 1dD thermo-fluid-mechanical analysis, are applied to perform the 2D thermal FEM Analysis of the thrust chamber wall.

Once the thermal problem is solved, the resulting thermal fields are then used as boundary conditions for different analyses of the wall, for the different chamber cross sections. The structural behavior of the combustion chamber wall under thermal and mechanical loads is investigated and the results are calculated in terms of Von Mises stresses. Finally, all the data are compared with those provided by Marc simulation software. The Shaped C results of the TS\_code will be compared both with Shaped C and Shaped O Marc solutions in order to detect how reliable the TS\_code is and the error introduced by the Shaped C geometry simplification.

## 3. The Matrix Displacement Method

The TS\_Code relies the resolution of the thermo-structural problem to the Matrix Displacement Method.

For an analytical determination of the distribution of static or dynamic displacements and stresses in a structure under prescribed external loading and temperature, we must obtain a solution to the basic equations of the theory of elasticity, satisfying the imposed boundary conditions on forces and/or displacements.

These equations are listed below, with the number of equations for a general three-dimensional structure in parentheses:

Strain-displacement equations	(6)
Stress-strain equations	(6)
Equations of equilibrium (or motion)	(3)

Thus there are fifteen equations available to obtain solutions for fifteen unknown variables, three displacements, six stresses, and six strains. For our two-dimensional problems we have eight equations with two displacements, three stresses, and three strains. Additional equations pertain to the continuity of strains and displacements (compatibility equations) and to the boundary conditions on forces and/or displacements.

### 3.1 Structure Discretization

The most important step in matrix structural analysis is the formulation of a discrete-element mathematical model equivalent to the actual continuous structure. This model is necessary in order to have a system with a finite number of degrees of freedom upon which matrix algebra operations can be performed. The formulation of such a model, usually referred to as structural idealization, is accomplished essentially by equating energies of the continuous and discrete element systems. If the elements are made up with fictitious boundaries and attachments, exact discrete element representations are not possible, and we must resort to the use of assumed displacement distributions within the elements. The assumed distributions must be such that when the size of elements is decreased, the matrix solutions for the stresses and displacements must tend to the exact values for the continuous system [3].

So, the structure is first idealized into an assembly of structural elements that are attached to the adjacent elements at node points, which in our case are the actual joints obtained by the intersecting grid lines. A form of displacement distribution is assumed for the discrete structural elements, and the complete solution of the equations of elasticity is then obtained by combining these individual approximate displacement distributions in a manner which satisfies the force-equilibrium and displacement compatibility at the junctions of these elements.

The fundamental step in the application of the matrix displacement method is the determination of the stiffness characteristics of structural elements into which the structure is idealized for the purpose of the analysis. A number of alternative methods are available for the calculation of force-displacement relationships describing the stiffness characteristics of structural elements, and the choice of a particular method depends mainly on the type of element. In this work the "Unit-displacement theorem" has been adopted for the calculation of the stiffness characteristics. This choice is due to the application of the unit-displacement theorem that is undoubtedly the most convenient since it leads directly to the required matrix equation relating element forces to their corresponding displacements [3].

### 3.2 Element Stiffness Properties by the Unit-Displacement Theorem

We shall consider an elastic element subjected to a set of  $n$  forces  $\mathbf{S} = \{S_1, S_2, \dots, S_i, S_j, \dots, S_n\}$  and some specified temperature distribution  $T = T(x, y, z)$ . The displacements corresponding to the forces  $\mathbf{S}$  will be denoted by the column matrix  $\mathbf{u} = \{u_1, u_2, \dots, u_i, u_j, \dots, u_n\}$ . To determine a typical force  $S_i$  we have used the unit-displacement theorem. Hence:

$$S_i = \int_v \boldsymbol{\varepsilon}_i^T \boldsymbol{\sigma} dV \quad (1)$$

where  $\boldsymbol{\varepsilon}_i$  represents the matrix of compatible strains due to a unit displacement in the direction of  $S_i$  and  $\boldsymbol{\sigma}$  is the exact stress matrix due to the applied forces  $\mathbf{S}$  and the temperature  $T$ . The unit displacements can be applied in turn at all points where the forces are impressed, and hence:

$$\mathbf{S} = \int_v \boldsymbol{\varepsilon}^T \boldsymbol{\sigma} dV \quad (2)$$

where  $\boldsymbol{\varepsilon} = [\boldsymbol{\varepsilon}_1 \boldsymbol{\varepsilon}_2 \dots \boldsymbol{\varepsilon}_i \boldsymbol{\varepsilon}_j \dots \boldsymbol{\varepsilon}_n]$ . Since we are dealing with a linear system, the total strains  $\mathbf{e}$  must be expressed by the relationship  $\mathbf{e} = \mathbf{b}\mathbf{u}$ , where  $\mathbf{b}$  represents a matrix of the *exact* strains due to unit displacements  $\mathbf{u}$ . Adopting plain strain hypothesis we can write:

$$\boldsymbol{\sigma} = \boldsymbol{\chi}\mathbf{b}\mathbf{u} + \boldsymbol{\chi}_T\alpha T \quad (3)$$

where

$$\boldsymbol{\chi} = \frac{E}{(1+\nu)(1-2\nu)} \begin{bmatrix} 1-\nu & \nu & 0 \\ \nu & 1-\nu & 0 \\ 0 & 0 & \frac{1-2\nu}{2} \end{bmatrix} \quad (4)$$

$$\boldsymbol{\chi}_T = \frac{E}{1-2\nu} \{-1 \quad -1 \quad 0\} \quad (5)$$

$E$  represents the Young Modulus,  $\nu$  is the Poisson ratio, and  $\alpha$  is the thermal expansion coefficient. Hence from Eqs. (2) and (3) the element force-displacement relationship becomes

$$\mathbf{S} = \int_v \boldsymbol{\varepsilon}^T \boldsymbol{\chi}\mathbf{b} dV \mathbf{u} + \int_v \boldsymbol{\varepsilon}^T \boldsymbol{\chi}_T \alpha T dV \quad (6)$$

$$\text{or } \mathbf{S} = \mathbf{k}\mathbf{u} + \mathbf{Q} \quad (7)$$

$$\text{where } \mathbf{k} = \int_v \boldsymbol{\varepsilon}^T \boldsymbol{\chi}\mathbf{b} dV \quad (8)$$

represents the element stiffness matrix and

$$\mathbf{Q} = \int_v \boldsymbol{\varepsilon}^T \boldsymbol{\chi}_T \alpha T dV \quad (9)$$

represents thermal forces on the element when  $\mathbf{u}=\mathbf{0}$ . If the temperature throughout the element is constant, then

$$\mathbf{Q} = \mathbf{h}\alpha T \quad (10)$$

$$\text{where } \mathbf{h} = \int_v \boldsymbol{\varepsilon}^T \boldsymbol{\chi}_T dV \quad (11)$$

may be described as the thermal stiffness matrix. Hence from Eqs. (7) and (10) we have

$$\mathbf{S} = \mathbf{k}\mathbf{u} + \mathbf{h}\alpha T \quad (12)$$

The matrix  $\boldsymbol{\varepsilon}$  representing compatible strain distribution can be evaluated without any appreciable difficulties, even for complex structural elements. On the other hand, evaluation of the matrix  $\mathbf{b}$ , representing exact strain distributions, is often exceedingly difficult, if not impossible. In cases for which no exact strain distribution can be found

approximate procedures must be used. This requires determination of approximate functional relationships between strains and displacements. Naturally, the degree of approximation then depends on the extent to which the equations of equilibrium and compatibility are satisfied. One possible approach is to select the matrix  $\mathbf{b}$  in such a way that it will satisfy only the equations of compatibility. Denoting this approximate matrix by  $\underline{\mathbf{b}}$ , and noting that  $\boldsymbol{\varepsilon} = \underline{\mathbf{b}}$ , we obtain from Eq. (8) [3]:

$$\mathbf{k} \simeq \int_v \underline{\mathbf{b}}^T \boldsymbol{\chi} \underline{\mathbf{b}} dV \quad (13)$$

For a convenience in subsequent analysis Eq. (11) may be rewritten as

$$\mathbf{h} = \int_v \underline{\mathbf{b}}^T \boldsymbol{\chi}_T dV \quad (14)$$

### 3.3 Rectangular Plate Elements (In-Plane Forces)

For the aim of our code, a rectangular plate element has been adopted for simplicity to discretize the structure.

The origin of the local coordinate system has been chosen properly and to simplify subsequent analysis nondimensional coordinates  $\xi = x/a$  and  $\eta = y/b$  have been introduced, where  $a$  and  $b$  are the dimensions of the rectangular plate. The element displacements are represented by the displacements  $u_1, u_2, \dots, u_8$ , and their positive directions are the positive directions of the  $x$  and  $y$  axes. Simple displacement functions which satisfy the assumption of linearly varying boundary displacements have been taken as:

$$u_x = c_1\xi + c_2\xi\eta + c_3\eta + c_4 \quad (15)$$

and

$$u_y = c_5\xi + c_6\xi\eta + c_7\eta + c_8 \quad (16)$$

where the arbitrary constants  $c_1, \dots, c_8$  are determined from the known displacements in the  $x$  and  $y$  directions at the four corners of the rectangle. Thus, the assumed displacement distribution is represented by a second-degree surface, where for constant values of  $\xi$  (or  $\eta$ ) the variation of displacement in the direction of  $\eta$  (or  $\xi$ ) is linear.

The following boundary conditions are used to evaluate the unknown constants  $c_1, \dots, c_8$ :

$$\begin{array}{lll} u_x = u_1 & \text{and} & u_y = u_2 \quad \text{at } (0,0) \\ u_x = u_3 & \text{and} & u_y = u_4 \quad \text{at } (0,1) \\ u_x = u_5 & \text{and} & u_y = u_6 \quad \text{at } (1,1) \\ u_x = u_7 & \text{and} & u_y = u_8 \quad \text{at } (1,0) \end{array} \quad (17)$$

Substituting these boundary values into the equations for displacements, we determine the unknown constants  $c_1, \dots, c_8$ ; hence:

$$u_x = (1 - \xi)(1 - \eta)u_1 + (1 - \xi)\eta u_3 + \xi\eta u_5 + \xi(1 - \eta)u_7 \quad (18)$$

$$u_y = (1 - \xi)(1 - \eta)u_2 + (1 - \xi)\eta u_4 + \xi\eta u_6 + \xi(1 - \eta)u_8 \quad (19)$$

Examining the form of Eqs. (18) and (19), we can see that the distribution of the  $u_x$  and  $u_y$  displacements along any edge is linear and that it depends only on the element displacements of the two corner points defining the particular edge. Thus, the assumed form of the displacement distribution ensures that the compatibility of displacements on the boundaries of adjacent elements is satisfied.

The total strains corresponding to the assumed displacement functions can be obtained by differentiation of Eqs. (18) and (19). Noting that

$$e_{xx} = \frac{\partial u_x}{\partial x} = \frac{1}{a} \frac{\partial u_x}{\partial \xi} \quad (20)$$

$$e_{yy} = \frac{\partial u_y}{\partial y} = \frac{1}{b} \frac{\partial u_y}{\partial \eta} \quad (21)$$

$$e_{xy} = e_{yx} = \frac{\partial u_y}{\partial x} + \frac{\partial u_x}{\partial y} = \frac{1}{b} \frac{\partial u_x}{\partial \eta} + \frac{1}{a} \frac{\partial u_y}{\partial \xi} \quad (22)$$

we find that the total strain-displacement relationship for the rectangular plate becomes

$$\mathbf{e} = \begin{bmatrix} e_{xx} \\ e_{yy} \\ e_{xy} \end{bmatrix} = \begin{bmatrix} -\frac{1-\eta}{a} & 0 & -\frac{\eta}{a} & 0 & \frac{\eta}{a} & 0 & \frac{1-\eta}{a} & 0 \\ 0 & -\frac{1-\xi}{b} & 0 & \frac{1-\xi}{b} & 0 & \frac{\xi}{b} & 0 & -\frac{\xi}{b} \\ -\frac{1-\xi}{b} & -\frac{1-\eta}{a} & \frac{1-\xi}{b} & -\frac{\eta}{a} & \frac{\xi}{b} & \frac{\eta}{a} & -\frac{\xi}{b} & \frac{1-\eta}{a} \end{bmatrix} \begin{bmatrix} u_1 \\ u_2 \\ u_3 \\ u_4 \\ u_5 \\ u_6 \\ u_7 \\ u_8 \end{bmatrix} \quad (23)$$

or, in using matrix symbolism,

$$\mathbf{e} = \mathbf{b}\mathbf{u} \quad (24)$$

where

$$\mathbf{b} = \begin{bmatrix} -\frac{1-\eta}{a} & 0 & -\frac{\eta}{a} & 0 & \frac{\eta}{a} & 0 & \frac{1-\eta}{a} & 0 \\ 0 & -\frac{1-\xi}{b} & 0 & \frac{1-\xi}{b} & 0 & \frac{\xi}{b} & 0 & -\frac{\xi}{b} \\ -\frac{1-\xi}{b} & -\frac{1-\eta}{a} & \frac{1-\xi}{b} & -\frac{\eta}{a} & \frac{\xi}{b} & \frac{\eta}{a} & -\frac{\xi}{b} & \frac{1-\eta}{a} \end{bmatrix} \quad (25)$$

$$\text{and } \mathbf{u} = \{u_1, u_2, \dots, u_8\} \quad (26)$$

Introducing Eq. (23) into plain strain formulation gives the following stress-displacement relationship:

$$\begin{bmatrix} \sigma_{xx} \\ \sigma_{yy} \\ \sigma_{xy} \end{bmatrix} = \frac{E}{1-\nu^2} \begin{bmatrix} \dots \\ \vdots \\ \ddots \\ \vdots \\ \dots \end{bmatrix} \begin{bmatrix} u_1 \\ u_2 \\ u_3 \\ u_4 \\ u_5 \\ u_6 \\ u_7 \\ u_8 \end{bmatrix} - \frac{E\alpha T}{1-\nu} \begin{bmatrix} 1 \\ 1 \\ 0 \end{bmatrix} \quad (27)$$

where the matrix within square parenthesis only depends upon  $E$ ,  $\nu$ ,  $\xi$ ,  $\eta$ ,  $a$  e  $b$ . From Eq. (23) it is evident that for a given set of displacements  $\mathbf{u}$  the  $e_{xx}$  strains are constant in the  $x$  direction ( $\xi$  direction) and that they vary linearly with  $y$  ( $\eta$  coordinate). Similarly, the  $e_{yy}$  strains are constant in the  $y$  direction, and they vary linearly with  $x$  ( $\xi$  direction). The shearing strains  $e_{xy}$ , on the other hand, vary linearly with both  $x$  and  $y$  ( $\xi$  and  $\eta$ ). If the temperature of the element is assumed constant, it follows from Eq. (27) that all stress components in the panel vary linearly with  $x$  and  $y$  and that the stress distributions is such that, in general, it violates the stress-equilibrium equations within the rectangle.

Calculation of the stiffness matrix  $\mathbf{k}$  and thermal stiffness  $\mathbf{h}$  requires integration with respect to  $\xi$  and  $\eta$  since the matrix  $\mathbf{b}$  is a function of the position variables. Substituting Eqs. (25) and (4) into (14), multiplying out the matrix product  $\mathbf{b}^T \boldsymbol{\chi} \mathbf{b}$ , and then integrating over the volume of the plate gives the stiffness matrix of Eq.(28).

$$\mathbf{k} = \frac{Et}{12(1-\nu^2)} \begin{bmatrix} \dots \\ \vdots \\ \ddots \\ \vdots \\ \dots \end{bmatrix}, \quad (28)$$

where the matrix within square parenthesis represents a  $8 \times 8$  symmetric matrix, only depending upon  $\beta$  and  $\nu$ . Similarly, substituting Eqs. (25) and (5) into (14), multiplying out the matrix product  $\mathbf{b}^T \boldsymbol{\chi}_T$ , and then integrating over the whole volume of the plate, gives for the thermal stiffness  $\mathbf{h}$

$$\mathbf{h} = \frac{E\alpha t}{2(1-\nu)} \{\beta \quad 1 \quad \beta \quad -1 \quad -\beta \quad -1 \quad -\beta \quad 1\} \quad (29)$$

### 3.4 Matrix Formulation of the Displacement Analysis

To determine the displacements of the idealized structure under some specified external loading and temperature distribution, we have obtained stiffness properties of the assembled structure made up from the idealized elements. In this paragraph we shall discuss how the stiffness matrices for individual elements has been combined to form the matrix equation relating the applied mechanical forces and equivalent thermal forces to the corresponding displacements on the assembled structure. Since the displacements appear as the unknowns, this formulation is, therefore, described as the matrix displacement method.

The fundamental assumption used in the analysis is that the structure can be satisfactorily represented by an assembly of discrete elements having simplified elastic properties and that these elements are interconnected so as to represent the actual continuous structure. The boundary displacements are compatible at least at the node points, where the elements are joined, and the stresses within each element are equilibrated by a set of element forces  $\mathbf{S}_n^{(i)}$  in the directions of element displacements  $\mathbf{u}_n^{(i)}$ . The element forces are related to the corresponding displacements by the matrix equation

$$\mathbf{S}_n^{(i)} = \mathbf{k}_n^{(i)} \mathbf{u}_n^{(i)} + \mathbf{Q}_n^{(i)} \quad (30)$$

where the superscript (i) denotes the *i*th element and all matrices refer to a datum coordinate system. Equation (30) can be determined for each element separately, and for the complete structure all these equations have been combined into a single matrix equation of the form

$$\mathbf{S}_n = \mathbf{k}_n \mathbf{u}_n + \mathbf{Q}_n \quad (31)$$

$$\text{where } \mathbf{S}_n = \{\mathbf{S}_n^{(1)} \quad \mathbf{S}_n^{(2)} \quad \dots \quad \mathbf{S}_n^{(i)} \quad \dots\} \quad (32)$$

$$\mathbf{k}_n = \{\mathbf{k}_n^{(1)} \quad \mathbf{k}_n^{(2)} \quad \dots \quad \mathbf{k}_n^{(i)} \quad \dots\} \quad (33)$$

$$\mathbf{u}_n = \{\mathbf{u}_n^{(1)} \quad \mathbf{u}_n^{(2)} \quad \dots \quad \mathbf{u}_n^{(i)} \quad \dots\} \quad (34)$$

$$\mathbf{Q}_n = \{\mathbf{Q}_n^{(1)} \quad \mathbf{Q}_n^{(2)} \quad \dots \quad \mathbf{Q}_n^{(i)} \quad \dots\} \quad (35)$$

It should be noted here that in the previous paragraph all matrices pertaining to individual elements were used without superscripts indicating the element number.

For subsequent analysis it is convenient to introduce a matrix of displacements on the assembled structure

$$\mathbf{U} = \{U_1 \quad U_2 \quad \dots \quad U_j \quad \dots \quad U_m\} \quad (36)$$

where  $U_j$  represents a typical nodal displacement, referred to a datum coordinate system.

The external loading corresponding to the displacements  $\mathbf{U}$  will be denoted by the matrix  $\mathbf{P}$ , such that

$$\mathbf{P} = \{P_1 \quad P_2 \quad \dots \quad P_j \quad \dots \quad P_m\} \quad (37)$$

where  $P_j$  represents an external force in the direction of the displacement  $U_j$ . To relate the external forces  $\mathbf{P}$  to the corresponding displacements  $\mathbf{U}$  virtual displacements  $\delta\mathbf{U}$  are introduced in a proper way [3]. From the principle of virtual work it follows that:

$$\mathbf{K}\mathbf{U} = \mathbf{P} - \mathbf{Q} \quad (38)$$

where  $\mathbf{K}$  is the stiffness matrix for the complete structure regarded as a free body and Eq. (38) represents equations of equilibrium for element forces acting at all joints. This implies that the load matrix  $\mathbf{P}$  must constitute a set of forces in static equilibrium, and it includes the reaction forces. However, all these forces are not independent. From the consideration of overall equilibrium of the structure it is clear that there must be six dependent equations, corresponding to the six rigid-body degrees of freedom, relating the forces  $\mathbf{P}$ . This is accomplished by assuming that six displacements at certain selected points on the structure are equal to zero and eliminating the corresponding rows and columns from the complete stiffness matrix  $\mathbf{K}$ . So, only introducing proper boundary conditions it has been possible to obtain the solution for displacements from

$$\mathbf{U}_r = \mathbf{K}^{-1}(\mathbf{P}_r - \mathbf{Q}_r) \quad (39)$$

where the subscript r is used to indicate that all matrices have been reduced in size to exclude forces and displacements at the selected points.

The calculation of the stiffness matrix  $\mathbf{K}$  has been carried out by placing elements from  $\mathbf{k}_n^i$  in their correct positions in the larger framework of the matrix  $\mathbf{K}$  and then summing all the overlapping terms.

The same procedure has been carried out for the calculation of the matrix  $\mathbf{Q}$  [3].

### 3.5 Thermal Problem Field

As we understood from the previous paragraph the temperature field is an input for the thermo-structural problem resolution. So, we first solved the thermal problem and then we faced the thermo-structural one.

To find the solution of thermal problem the analysis has been based on thermal finite elements. So, the virtual temperature principle has been involved thank to Mathematica language subroutine. The principle is in close analogy with the virtual work principle, so that for what concern the state variables we can refer to the following analogy:

- Displacements  $u_i \rightarrow T$  Temperature
- Strains  $\epsilon_{ij} \rightarrow T_{,i}$  Temperature gradient
- Stresses  $\sigma_{ij} \rightarrow q_i$  Heat Flux

For what concerns the loads, instead, we can refer to the following analogy:

- Internal Loads (per unit volume)  $X_i \rightarrow q_{gen}$  Generated Heat (per unit volume per unit time)
- Surface Loads (per unit area)  $f_i \rightarrow q_{ii}$  Thermal flux on  $S_q$
- Prescribed Displacements  $u_{ii} \rightarrow T_{ii}$  Prescribed Temperatures on  $S_T$

For the governing equations, the following similitude can be written:

- Equilibrium  $\sigma_{ij,j} + X_i = 0 \rightarrow -q_{i,i} + q_{gen} = 0$
- Compatibility  $\epsilon_{ij,j} = 1/2 \text{ left}(u_{i,j} + u_{j,i}) \rightarrow \text{grad}T = T_{,i}$
- Constitutive  $\sigma_{ij} = C_{ijhk} \epsilon_{hk} \rightarrow q_i = -\lambda T_{,i}$

By solving the the virtual temperature principle for a steady state case, we have been able to find the temperature field  $T(x,y)$  within the structure.

## 4. The Simulations Results

The simulations activities have been performed to compare the TS\_code results with those provided by Marc both for Shaped C and Shaped O geometries. The dimensions used are based on an AVIO combustion chamber really developed, manufactured and tested where the material for the liner is copper allow while the close-out is based on Inconel. Different cases have been analyzed by varying the cross section analyzed (chamber or divergent cross sections) and the boundary conditions (proof and hot firing conditions). The next table summarizes the cases studied for the comparison.

Table 1: Case studied for the simulation activity

	LOAD	MODEL	P [bar]	GEOMETRY	SECTION
<b>CASE 1</b>	Proof	Linear	Pcool = 200	TS_Code - Shaped C Marc - Shaped C Marc - Shaped O	Chamber
<b>CASE 2</b>	Proof	Linear	Pcool = 200	TS_Code - Shaped C Marc - Shaped C Marc - Shaped O	Divergent
<b>CASE 3</b>	Firing	Linear	Pcc = 55	TS_Code - Shaped C Marc - Shaped C Marc - Shaped O	Chamber

#### 4.1 Mesh and Global Stiffness Matrix

For a correct comparison the same geometry discretization has been kept between TS\_Code and Marc. The number of elements chosen has been set properly, for a converging solution. Here we recall that high effort has been spent to find the right way to assemble the stiffness matrix. In fact, a well-banded global stiffness matrix guarantees the correct way for a stable and reliable solution. Next figure shows the typical mesh used for the cases above mentioned and typical form of well-banded global stiffness matrix, both obtained with the TS\_Code.

The number of elements used is equal to 160, that corresponds to a number of variable equal to 322.

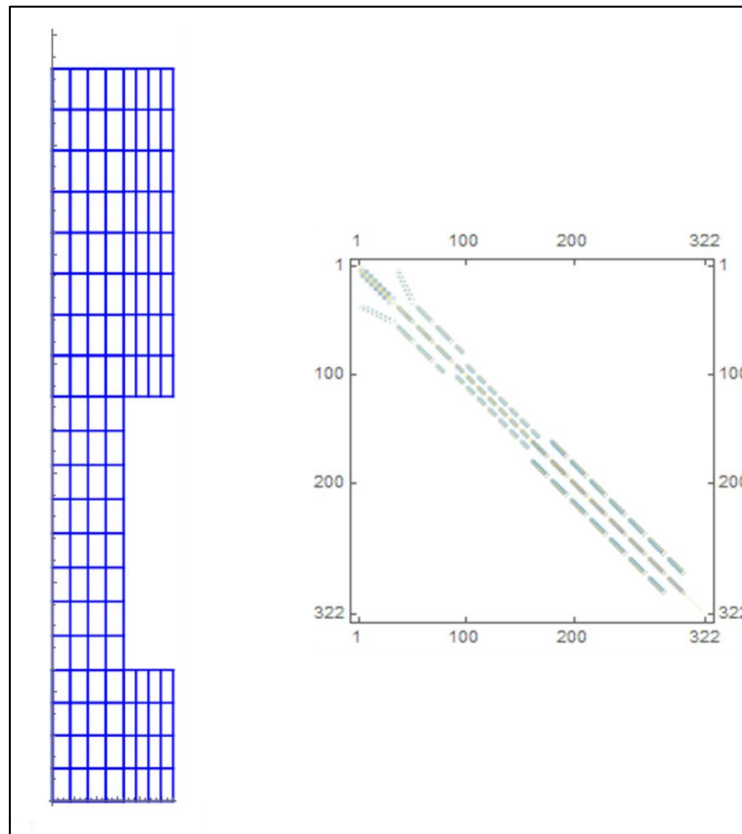


Figure 6: Mesh and global stiffness matrix obtained by TS\_Code

#### 4.2 Case 1 and Case 2 Results Comparison

In this section the results of comparison between the results obtained with the TS\_Code (based on Mathematica programming language) and those provided by Marc simulation software, regarding the first and second test cases will be shown.

These two cases regard typical proof test conditions of thrust chamber where the cooling jacket is pressurized while no combustion takes place in the chamber, so that the pressure is equal to ambient one.

As we can see from Figure 7 and Figure 8, the Shaped C structure undergoes displacements towards negative direction of y axis, in opposition to what occur for the Shaped O structure. This is due to different boundary conditions set at the upper part of the structure. For Shaped C structure fixed conditions have been set, while for the Shaped O geometry ambient pressure acting on the surface has been imposed.

The maximum stress field is reached in proximity of the rib. As we can note the plot solutions of Marc and TS\_Code Shaped C geometry are very similar. The spike detected on the TS\_Code solution is not realistic since it occurs at the square corner of the cooling channel. For a more realistic comparison we refer to Figures 9 – 11, where the compared solutions refer to the variables trends occurring along the y axis for a fixed x axis value equal to a half of rib thickness.

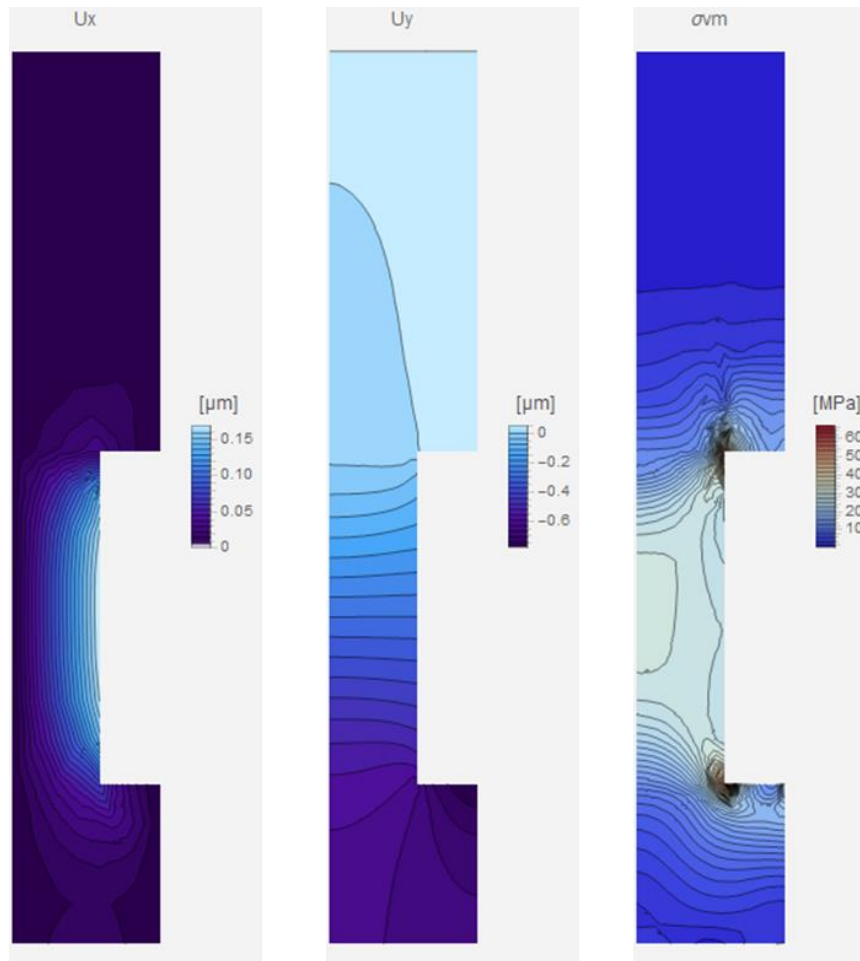


Figure 7: Plot of  $U_x$ ,  $U_y$  and  $\sigma_{VM}$  obtained by TS\_Code for Shaped C geometry for Case 1

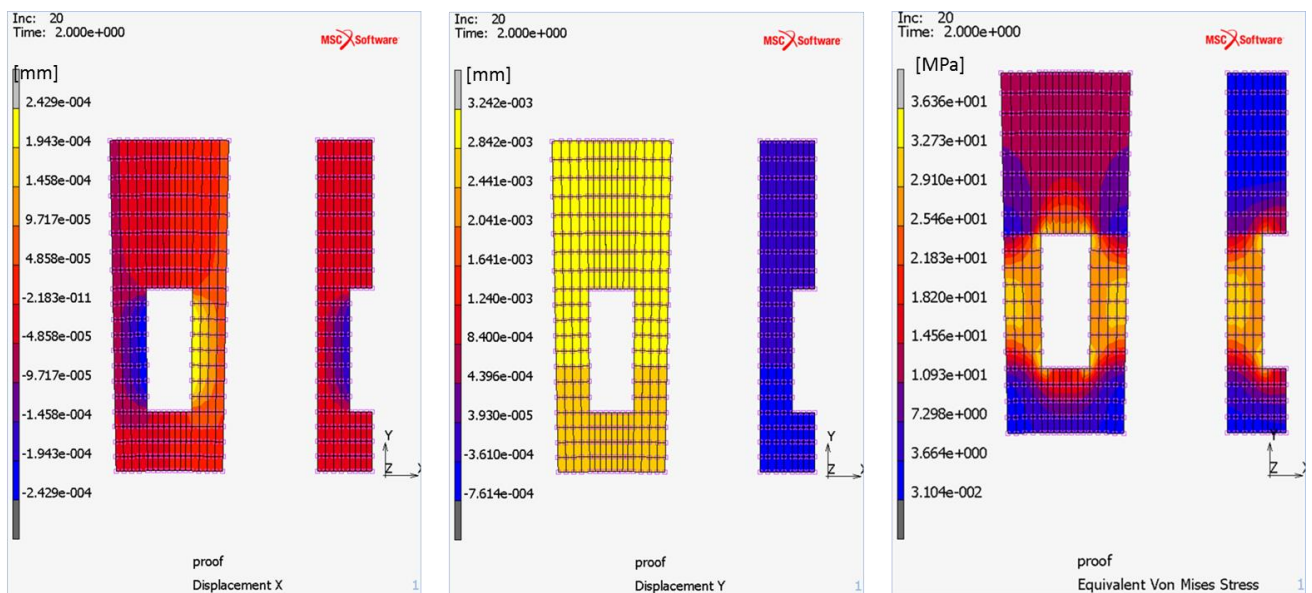
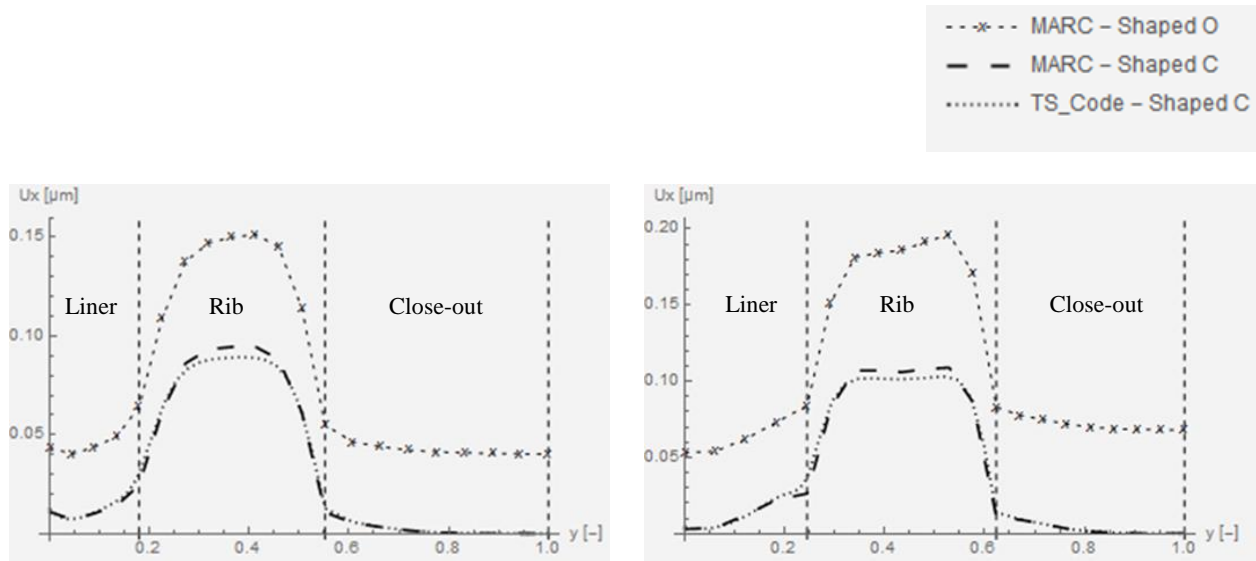
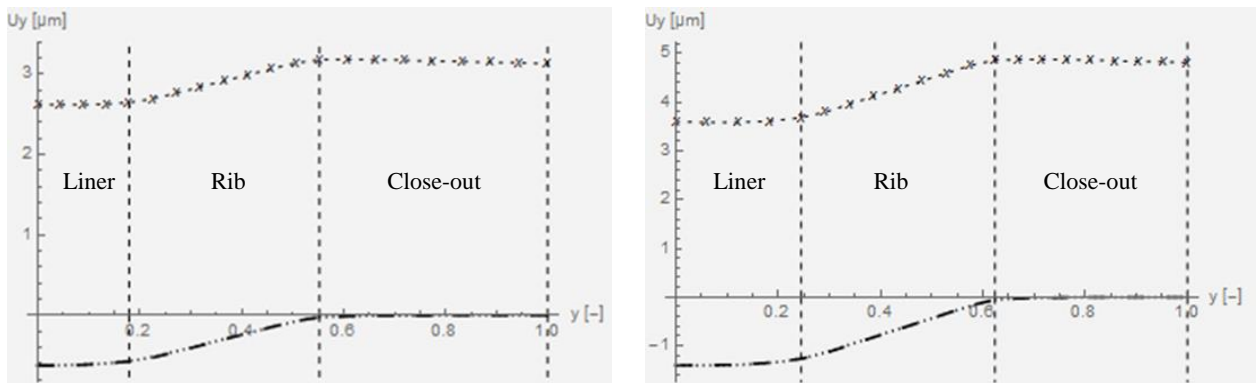
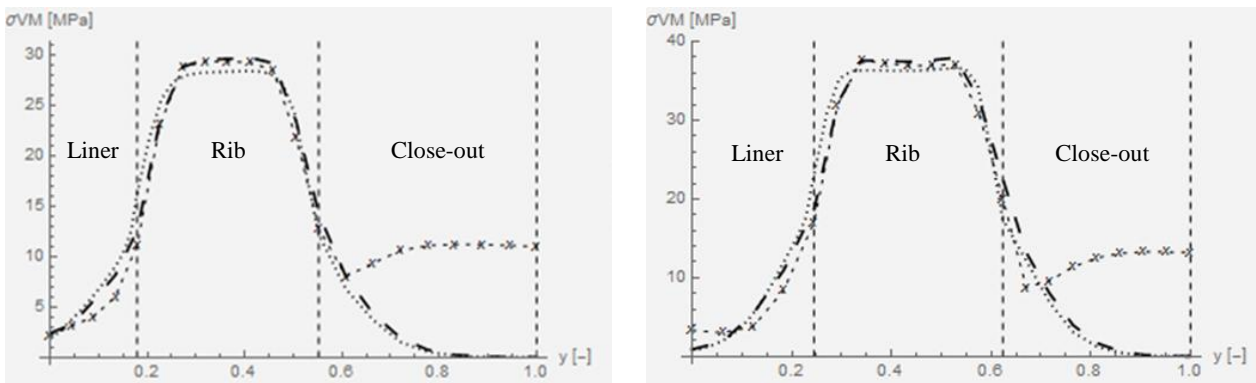


Figure 8: Plot of  $U_x$ ,  $U_y$  and  $\sigma_{VM}$  obtained by Marc for Shaped O (left side of figures) and Shaped C (right side of figures) geometries for Case 1

Figure 9: Plot of  $U_x$  along the structure - Case 1 (left side), Case 2 (right side)Figure 10: Plot of  $U_y$  along the structure - Case 1 (left side), Case 2 (right side)Figure 11: Plot of  $\sigma_{VM}$  along the structure - Case 1 (left side), Case 2 (right side)

As we can note from the figures above, the comparison between the Shaped C solutions are very close for all the analyzed variables both for Case 1 and Case 2. In particular, only in proximity of the rib a maximum error of 5 [%] is detected for the  $U_x$  displacements. For the  $U_y$  solutions an error of 0 [%] about is recorded while for the von mises stress the maximum is 3 [%] about. Also for what respect to Shaped O solution the stress are similar except for the close-out. For the other variables the qualitative trends of Shaped O solution is similar to Shaped C one. All the results shown have been obtained from a converging activity, not presented in this work.

### 4.3 CASE 3 Results Comparison

The plot solutions between Marc and TS\_Code results are compared for the firing test conditions. As before the structure undergoes displacements toward the positive y direction for the Shaped C structure and towards negative one for the Shaped O geometry. The plot solution for Shaped C structures are very similar with respect of those provided by Marc. Also the temperature fields record the same trend. For a more comprehensive comparison in Figure 14 – 15 the trends detected in the middle of rib thickness are provided.

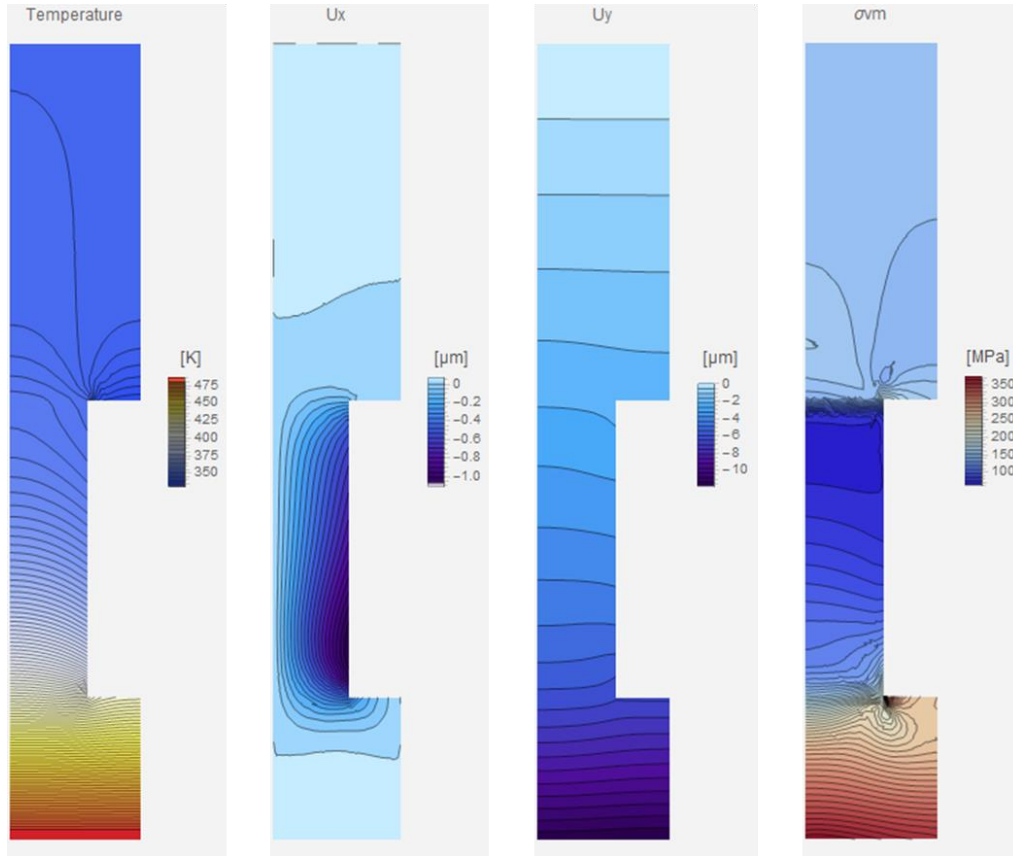


Figure 12: Plot of  $T$ ,  $U_x$ ,  $U_y$  and  $\sigma_{VM}$  obtained by TS\_Code for Shaped C geometry for Case 3

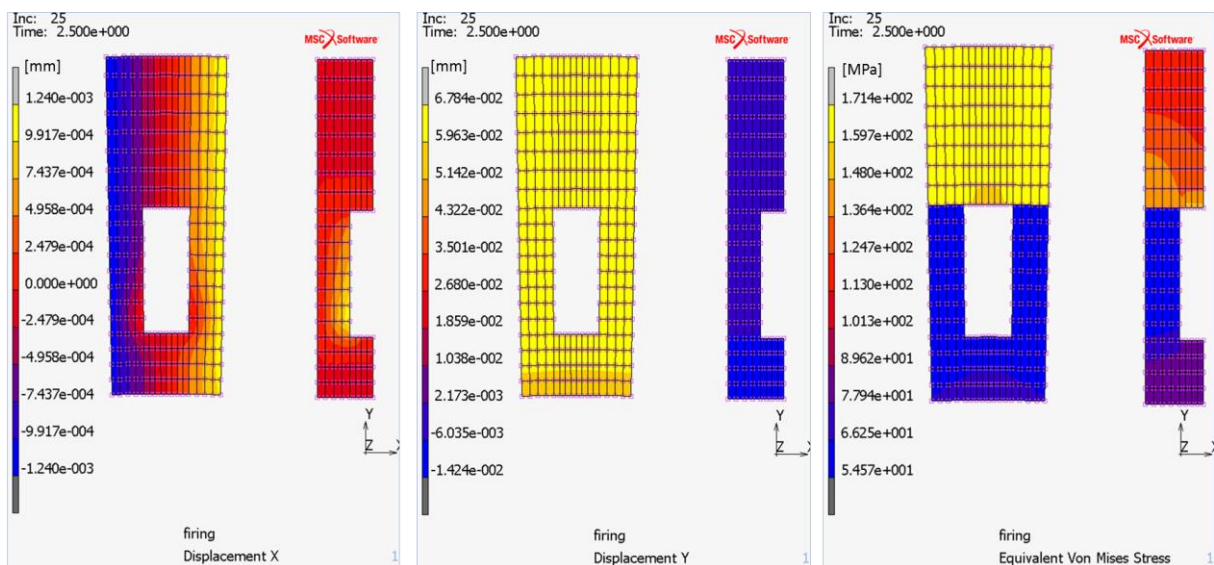
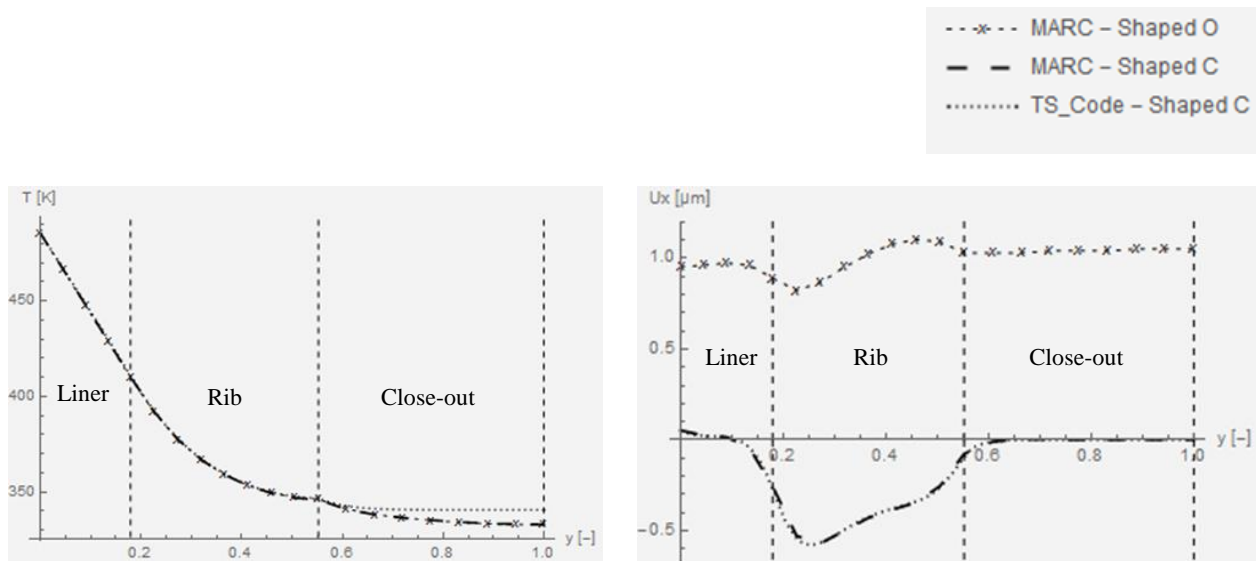
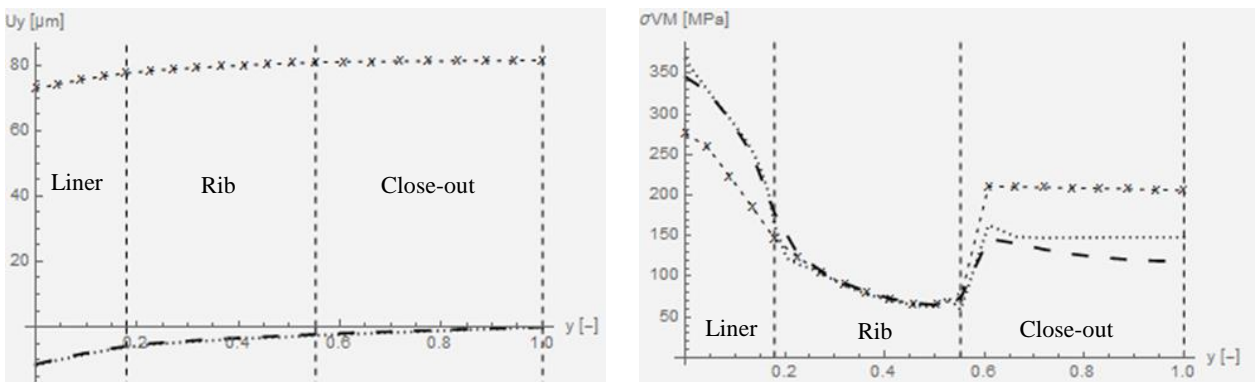


Figure 13: Plot of  $U_x$ ,  $U_y$  and  $\sigma_{VM}$  obtained by Marc for Shaped O (left side of figures) and Shaped C (right side of figure) geometries for Case 3

Figure 14: Plot of T (left side) and  $U_x$  (right side) along the structureFigure 15: Plot of T (left side) and  $U_x$  (right side) along the structure

As we can note from Figure 14 – 15, the two Shaped C solutions are very close each other for all the variables confirming that TS\_Code is a good tool to estimate Shaped C solution. In particular for  $U_x$  and  $U_y$  solutions the percentage errors are 0 [%] about. For the temperature the error reaches value of 3 [%] in the close-out. This difference has an impact on the stresses detected on close-out where the percentage error reached values higher than 10 [%].

With respect to Shaped O solution a good comparison is reached only for the temperatures. For the others variable only the qualitative trends tend to be similar to that provided by Shaped C solutions.

All the results shown have been obtained from a converging activity, not presented in this work.

## 5. Conclusions

AVIO is spending high effort in the designing of regenerative combustion chamber. A crucial point of the project is to dimension the combustion chamber walls. The current designing process foresees several loops between 1D thermo-fluid analysis and 3D Fem chamber simulations. This procedure requires a lot of time since the Fem analysis nowadays provided by the commercial software are not suitable for an optimization activity. In this framework the TS\_Code has been developed to answer to the necessity of reducing the number of 3D simulations. The TS\_code is based on the finite element analysis and has been written by means of Mathematica programming language. It is able to calculate the stresses solution within a 2D cross section of the chamber. The aim of the code is to optimize the combustion chamber dimensioning from the thermo-structural point of view, reducing the designing time. In the logic of a step by step code development, AVIO developed a first version of the code where some simplifications have been introduced. In particular, it is able to provide solution for a Shaped C geometry of the chamber cross

section. Moreover, the analysis is based on a linear approach. To ensure the efficiency of TS\_code first version, 3 comparisons have been carried out with the solutions provided by Marc programming software. In particular, chamber and divergent geometries have been tested under proof and firing test conditions. Moreover, a comparison with a real chamber cross section (Shaped O geometry) has been carried out to understand how much the Shaped C solution is different.

The results confirmed that TS\_Code is an efficient tool to solve the thermo-mechanical problem within Shaped C geometries of combustion chamber. With respect to Marc solutions, error percentages between 0 and 5 [%] have been detected both for proof and firing test conditions, except for the close-out in firing test conditions where higher values have been reached. This discrepancy is due in part to the error detected on the temperature.

For what concern the comparison with the realistic chamber cross section (Shaped O geometry), the solutions trends reached by the simplified geometry (Shaped C) are different, even though the qualitative trend is similar.

This shows that the Shaped C geometry is not a reliable geometry to describe the thermo-structural field within the chamber. In spite of that, the goodness of comparison between the Shaped C solutions ensure that TS\_Code model is robust and that it represents a reliable starting point for the development of a more realistic model where Shaped O geometry, as well as, unsteady and non linear analysis could be included for the future works.

### References

- [1] Kuhl, D., Riccius, J.R. and Haidn, O.J., "Thermo-mechanical analysis and optimization of cryogenic liquid rocket engines," *AIAA Journal of Propulsion and Power*, Vol. 18, No. 4, 2002, pp. 835-846.
- [2] "LRE Chamber Wall Optimization Using Plane Strain and Generalized Plane Strain Models" – Jörg R. Riccius, Evgeny B. Zametaev, Oskar J. Haidn, Christian Gogu – 42nd AIAA/ASME/SAE/ASEE Joint Propulsion Conference & Exhibit – 9 - 12 July 2006, Sacramento, California.
- [3] J.S. Przemienicki, *Theory of Matrix Structural Analysis*, Institute Senior Dean and Dean of Engineering Air Force Institute of Technology. Dover Publications, Inc. New York